Investigations of Some Physical Properties and Sensing Properties of Fluorine-Doped Alpha-Iron (III) Oxide Thin Films

Israa Akram Abbas[1], Oday Ali Chichan[2], Tahseen H. Mubarak[3], Shaymaa A. Hussein[4], Sami Salman Chiad[1], Nadir Fadhil Habubi [1,5,6] and Yassin Hasan Kadhim[7]

[1]*Department of Physics, College of Education, Mustansiriyah University, 10052 Baghdad, Iraq*
[2]*Department of Physics, College of Education for Pure Sciences, University of Babylon, 51001 Hillah, Babil, Iraq*
[3]*Department of Physics, College of Science, University of Diyala, 32001 Baqubah, Diyala, Iraq*
[4]*Department of Medical Laboratory Techniques, Al-Manara College for Medical Science, 62001 Al-Amarah, Maysan Governorate, Iraq*
[5]*Department of Radiation and Sonar Technologies, Alnukhba University College, 10013 Baghdad, Iraq*
[6]*Department of Radiology Techniques, Al-Qalam University College, 36001 Kirkuk, Iraq*
[7]*Department of Optics Techniques, College of Health and Medical Techniques, AL-Mustaqbal University, 51001 Hillah, Babylon, Iraq*
dean@sciences.uodiyala.edu.iq, dr.sami@uomustansiriyah.edu.iq, nadirfadhil@uomustansiriyah.edu.iq, yassin.hasan@uomus.edu.iq, shaimaa2021@uomanara.edu.iq, ssaakk02@uomustansiriyah.edu.iq

Keywords: Spray Pyrolysis, SPD, ZnS, In: ZnS, Optical, XRD, AFM, Band Gap Energy and Structural.

Abstract: Fluorine-doped α-Fe_2O_3 nanostructure films were synthesized by a facile Chemical Spray Pyrolysis (CSP) technique at a substrate temperature of 400 °C using standard glass slides. The fluorine dopant concentration was varied incrementally at 0%, 2%, and 4% by weight in order to systematically investigate its influence on the structural, morphological, and optical properties of the deposited films. X-ray diffraction (XRD) analyses exhibit well-defined diffraction peaks corresponding to the (017), (113), (119), and (220) planes, confirming the successful formation of the pure α-Fe_2O_3 (hematite) phase without any detectable secondary phases. The average crystallite size of hematite increased from 13.98 nm to 16.78 nm with rising fluorine content, indicating enhanced crystal growth and improved crystallinity due to doping. Atomic Force Microscopy (AFM) images reveal uniformly distributed grains with a smooth surface texture free of cracks or pinholes. Furthermore, the surface morphology and grain dimensions were noticeably altered as the dopant concentration increased. Optical characterization demonstrated a progressive decrease in transmittance with fluorine incorporation, reaching 65% at 600 nm, accompanied by a clear blue shift in the optical band gap, indicating modified electronic transitions and enhanced optical activity in the doped films..

1 INTRODUCTION

Hematite (α-Fe_2O_3), Because of its benefits and uses, has garnered a lot of interest [1]-[2], with band gap of (2.2-2.6) eV. [3]. Additionally, hematite's nontoxicity, affordability, environmental friendliness, and comparatively high stability make it an appealing material for all applications [4]. Doping with Cr, Zn, Ni, Ga, and Co at Fe site in hematite influences the physical properties [5]-[10]. The morphologies and structures of nanostructures have a significant impact on their unique characteristics. [11]-[19]. Fluorine doping into metal oxides has recently been the subject of numerous investigations in an effort to enhance the electrochemical outcomes of solar cells and lithium-ion batteries (LIBs) [18], [20-24].

2 EXPERIMENTAL DETAILS

Fluorine-doped α-Fe_2O_3 was prepared via CSP. O.1 M of $FeCl_3$, and NH_4F were settled via deionized water with a small amount of HCl drips. A weight ratio of 2% and 4% of Fluorine was carried out. The ideal conditions were as follows: base temperature of 400°C, spraying time of 8 s and pausing time of 1 min, air as a carrier gas set at a pressure of 10^5 pa,

and spout-to-base spacing of 28 cm. 310 ± 25 nm was the calculated film thickness using the gravimetric approach. The samples were studied by XRD. AFM was utilized to study deposited thin film surfaces. Transmittance spectra were achieved utilizing UV-Vis spectrophotometer. Gas sensitivity was done inside a cylindrical chamber with a radius of 10 cm and a height of 18 cm.

3 RESULTS AND DISCUSSIONS

Figure 1 depicts the XRD styles of the entended films. The peaks that were spotted. at 2θ: 24.62°, 31.14°, 37.82° and 62.71°correspond to (017), (113), (119) and (220) planes respectively. The measured reflections are classified based on the α-Fe_2O_3 phase's rhombohedral crystal structure. and reliable with ICDD (card no.40-1139) [25]. The (113) reflection was the most intense one. This shifting of XRD peaks results in lattice parameter variation as shown in Table 1. The host lattice's irregular distribution brought on by a larger F-ion content is mostly responsible for altering the different physical characteristics. After F-doping, the lattice parameter values undergo a change due to the reduced radius of F^- ions (1.33 Å) in comparison to O^{2-} ions (1.40 Å) [26].

The crystalline sizes (*D*) were calculated via (1) [27]:

$$D_{hkl} = \frac{0.9\lambda}{\beta cos\theta}, \quad (1)$$

where λ =1.54 Å, β is FWHM, and θ is Bragg angle.

Lattice strain (ε) and dislocation density (δ)formula were calculated using (2) [28]:

$$\varepsilon = \frac{\beta cos\theta}{4} \ (lines^{-2}.m^{-1}) \quad (2)$$

$$\delta = \frac{1}{D^2}\left(\frac{lines}{m^2}\right), \quad (3)$$

D is found in the range of 13.98-16.17nm. these findings agree with Mote et al. [29].

AFM pictures of α-Fe_2O_3 and doping in Fluorine nanostructure thin films are depict in Figure 3. The regular distribution of grain size is seen by the AFM images. of columnar aggregates without any cracks or holes. The average particle sizes P_{av} are: 87.2, 67.78 and 32.83 nm for 0, 2 and 4 wt.% respectively. The deposit surface roughness R_a ranged from (8.69 to 3.32) nm. P_{av} and root mean square roughness (rms) differ in roughness behaviour in undoing and doping. The system roughness is affected by various parameters, among which surface diffusion temperatures [30], [31].

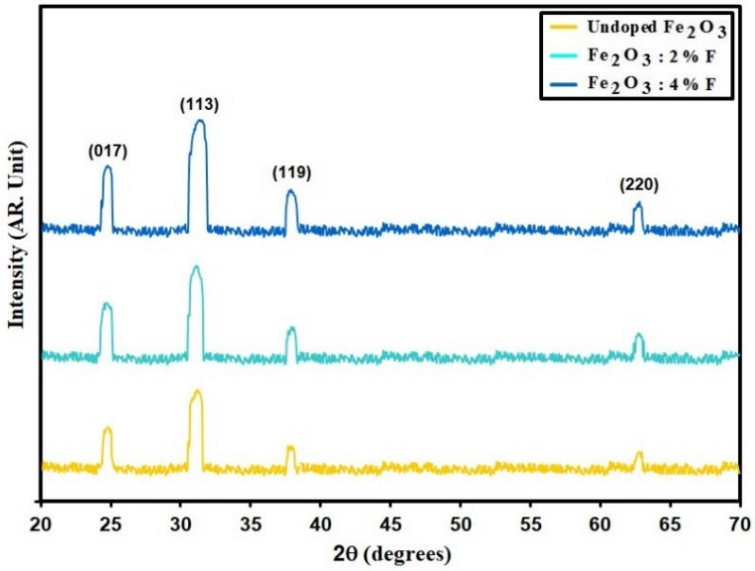

Figure 1: XRD styles of the entended films.

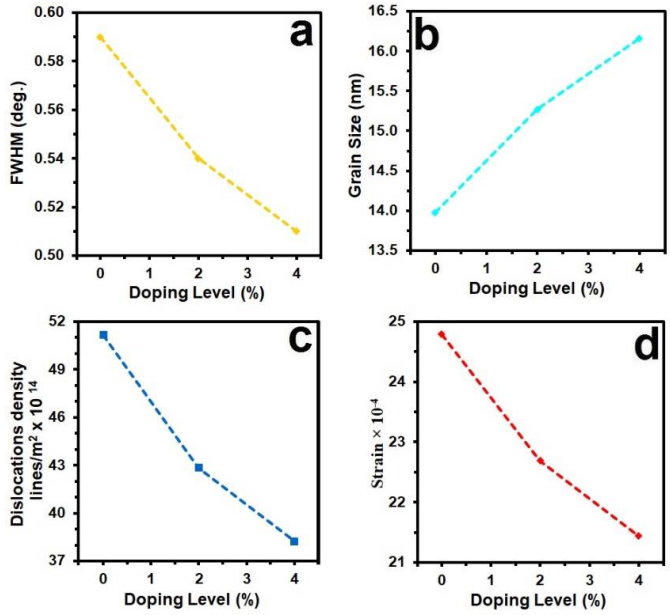

Figure 2: X-ray parameter of the deposit films.

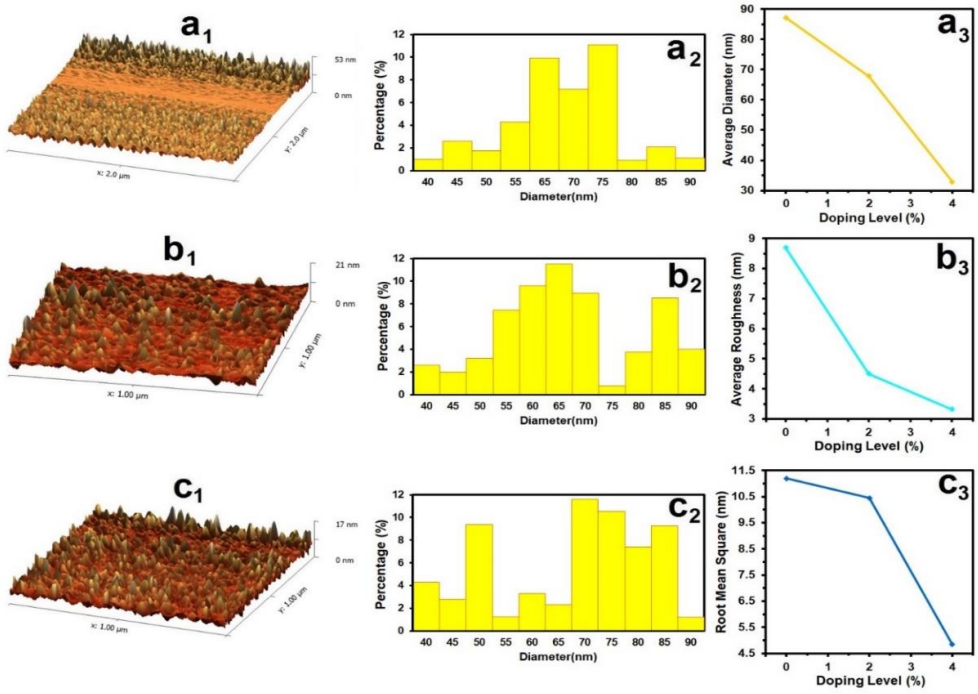

Figure 3: AFM information.

Figure 4, shows transmittance(T) of deposit films, optical transmission depending on the doping concentration. From the figure, the visible region's transmission is 65% to 75% . An increase in the doping concentration causes the transmittance to decrease and the absorbance to increase. This result is in agreement with Sivakumar et al. [32], [33].

Figure 5. offer the optical absorbance of pure and α-Fe_2O_3:F thin films. UV-Vis absorbance spectrum results show high optical absorption occurs at 380 nm [34], [35]. According to the UV-Vis absorbance spectrum, the absorption rate of the α-Fe2O3:F sample increases with the percentage increase in the Fluorine concentration.

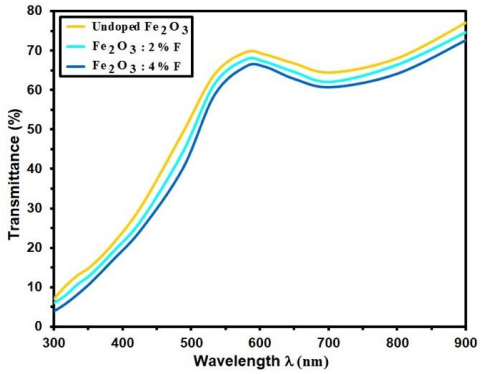

Figure 4**:** Transmittance of the deposit films.

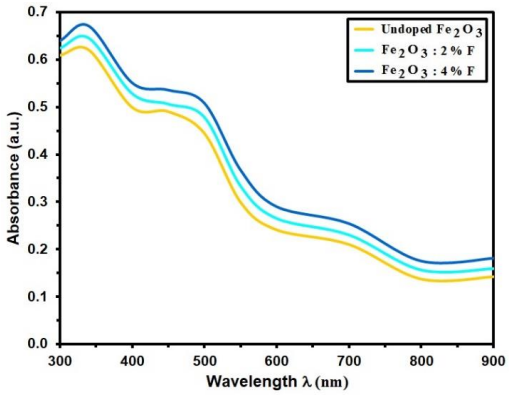

Figure 5: Absorbance of the deposit films.

The absorption coefficient α is measured by (4) [36]:

$$\alpha = \frac{\frac{1}{lnT}}{d} \quad (4)$$

where d is film thickness. Figure 6 shows α versus the photon energy ($h\nu$) of various doping of Al. Fluorine content. From Figure 7. ,it is evident that α increases easily with hν up to 2.42 eV, but for hν < 2.42 eV, α increases abruptly. A has high values (10^4 cm^{-1}) for all films, in addition to its value risen slightly as Fluorine content was increased [37].

Tauc's relation has been used to compute the band gap as follows: [38]:

$$\alpha h\nu = B(h\nu - E_g)^n \,, \quad (5)$$

B is a constant , hν photon energy and n is taken 1/2 for direct gap [39, 40]. Figure 7. shows E_g values determined as, A noticeable increase in E_g for doped films compared to the udoped ones, E_g = 2.48 eV for pure α-Fe_2O_3 and (2.42, 2.38) eV for Fluorine content at 2% and 4 wt.% respectively. The same phenomena are carried out in the literature [41,42]. The refractive index (n) was obtained by (6) [43]:

$$R = \frac{(n-1)^2}{(n+1)^2} \quad (6)$$

Where R is reflectance.

The extinction coefficient (k) is evaluated via (7) [44]:

$$k = \frac{\alpha\lambda}{4\pi}. \quad (7)$$

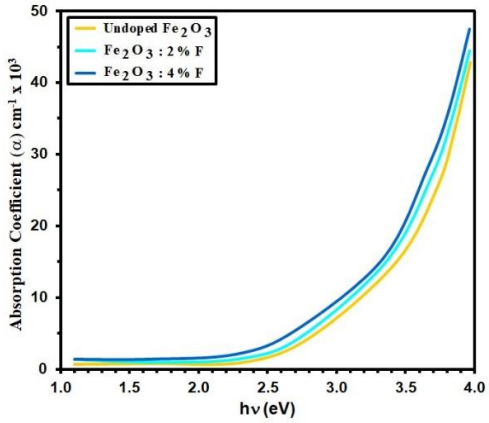

Figure 6: Absorption coefficient (α) Vs hν of the prepared films.

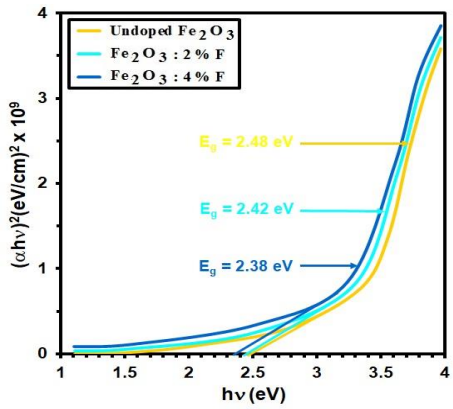

Figure 7: Plot of $(\alpha h\nu)^2$ versus hν for the Fe_2O_3 with different Fluorine doping.

Figure 8 shows n as a function of wavelength. It is discovered that raising the Fluorine doping content improves (n). The variation of n with wavelength in the range of (300-900) nm is dependent on the reflectance as shown by (6) Figure 9 shows the extinction coefficient of entended films. As can be seen from this figure, for all produced films, k falls dramatically with increasing wavelength up to 600 nm, and its value increases with increasing doping 45, 46. From Figure 8 k values increase with increased doping, which may be attributed to a change in crystalline structure. The

improved of crystalline development is the cause of this increase [47-50].

In Figure 10, the observed trend illustrates the resistance variation over time for entended films when exposed to 150 ppm of NO_2 at a temperature of 100°C. This behavior highlights the impact of NO_2 molecules in initiating surface oxidation. Specifically, this process involves the interaction between NO_2 and pre-adsorbed oxygen species (O_2^+ ions) [51-54], leading to the release of trapped electrons. These electrons subsequently migrate back to the CB, as a consequence, resistance rises. This phenomenon also enhances the potential barrier under these conditions. Notably, at a fluorine doping concentration of 4 wt.%, the Fe_2O_3 film exhibits the highest resistance (R). This suggests a direct correlation between fluorine doping and increased film sensitivity, as well as enhanced resistance to gas flow [55, 56]. The significant rise in resistance is attributable to the modification of charge carrier concentration and potential barrier height, which effectively influences the film's response to NO_2 exposure [57, 58]. The detection sensitivity, also referred to as the sensor response, can be calculated using the following (8) [59]:

$$Sensitivity = \frac{\Delta R}{R_g} = \left|\frac{R_g - R_a}{R_g}\right| \times 100\ \% \qquad (8)$$

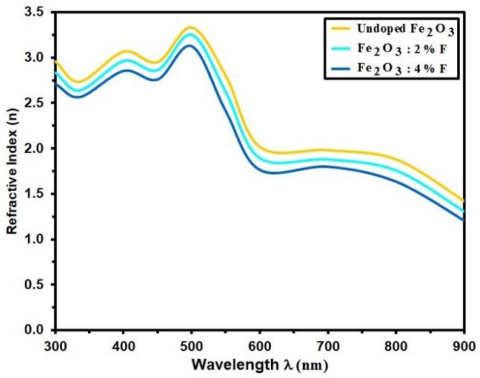

Figure 8: Refractive Index for grown films.

Figure 11 illustrates the variation in sensor sensitivity for undoped Fe_2O_3 and fluorine-doped Fe_2O_3 films with fluorine concentrations of 2 wt.% and 4 wt.% after exposed to NO_2 gas. The observed decrease in s with increasing fluorine doping is primarily attributed to charge carrier recombination [60]. This process occurs as electrons released from adsorbed oxygen species interact with holes in the Fe_2O_3 film, leading to a decrement in free charge carriers and, consequently, a rise in electrical resistance.

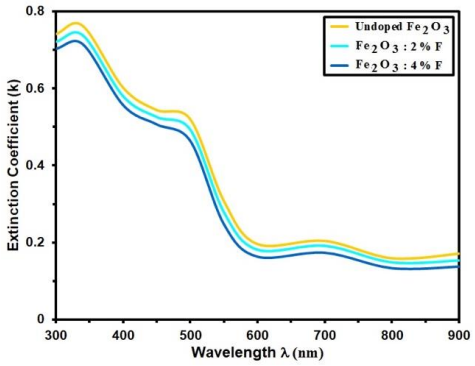

Figure 9: Extinction coefficient (k) of the grown films.

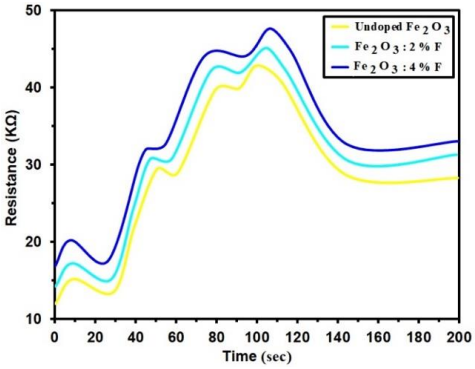

Figure 10: Dynamic Resistance of undoped Fe_2O_3 and Fluorine content at 2% and 4 wt.% respectively.

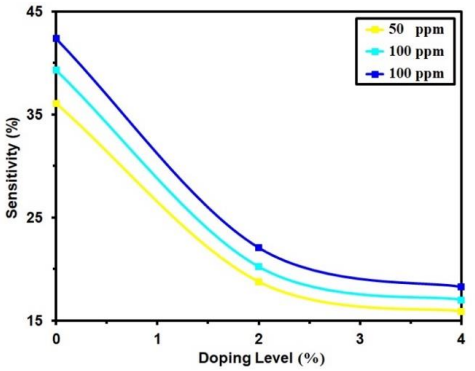

Figure 11: Sensitivity of undoped Fe_2O_3 and Fluorine content at 2% and 4 wt.% respectively.

4 CONCLUSIONS

Fluorine-doped α-Fe_2O_3 nanostructured thin films were successfully synthesized using the chemical spray pyrolysis (CSP) method at a substrate temperature of 400°C. Structural analysis through XRD confirmed the formation of the hematite phase

with no secondary phases. The crystallite size slightly increased from 13.98 nm to 16.17 nm with the increase in fluorine content.Surface morphology examined by AFM revealed uniformly distributed grains and smooth surfaces without cracks or pinholes. The root mean square (RMS) surface roughness decreased significantly with higher fluorine concentration. Optical analysis showed a decrease in transmittance and an increase in absorbance with increased fluorine content. The optical bandgap exhibited a slight blue shift, decreasing from 2.48 eV in pure films to 2.38 eV at 4% fluorine doping. This change is attributed to the formation of defect states and improved carrier transitions. Additionally, the refractive index and extinction coefficient increased with fluorine content. Gas sensing results demonstrated a notable increase in electrical resistance upon exposure to NO_2, especially in films doped with 4% fluorine. This suggests that fluorine doping enhances the potential barrier and sensitivity of the film. However, overall sensitivity decreased with increased fluorine content due to increased charge carrier recombination.

ACKNOWLEDGMENTS

The authors would like to express their gratitude to Mustansiriyah University and Alnukhba University College for their support.

REFERENCES

[1] M. Toghraei and H. Siadati, "Electrodeposited co-pi catalyst on α-Fe_2O_3 photoanode for water-splitting applications," International Journal of Engineering, Transactions C: Aspects, vol. 31, no. 12, pp. 2085-2091, 2018.

[2] K. D. Salman, "Synthesis and characterization unsaturated polyester resin nanocomposites reinforced by Fe_2O_3+Ni nanoparticles: Influence on mechanical and magnetic properties," International Journal of Engineering, Transactions A: Basics, vol. 35, no. 1, pp. 21-28, 2022.

[3] A. Boudjemaa, S. Boumazaa, M. Trari, R. Bouarab, and A. Bouguelia, "Physical and photo-electrochemical characterizations of α-Fe_2O_3 – application for hydrogen production," Int. J. Hydrogen Energy, vol. 34, pp. 4268-4274, 2009.

[4] N. Beermann, L. Vayssieres, S. E. Lindquist, and A. Hagfeldt, "Photoelectrochemical studies of oriented nanorod thin films of hematite," J. Electrochem. Soc., vol. 147, pp. 2456-2461, 2000.

[5] S. Shen, P. Guo, D. A. Wheeler, J. Jiang, S. A. Lindley, C. X. Kronawitter, J. Z. Zhang, L. Guo, and S. S. Mao, "Physical and photoelectrochemical properties of Zr-doped hematite nanorod arrays," Nanoscale, vol. 5, p. 9867, 2013.

[6] G. Wang, Y. Ling, D. A. Wheeler, K. E. N. George, K. Horsley, C. Heske, J. Z. Zhang, and Y. Li, "Facile synthesis of highly photoactive α-Fe_2O_3-based films for water oxidation," Nano Lett., vol. 11, pp. 3503-3509, 2011.

[7] M. Z. Dang, D. G. Rancourt, J. E. Dutrizac, G. Lamarche, and R. Provencher, "Interplay of surface conditions, particle size, stoichiometry, cell parameters, and magnetism in synthetic hematite-like materials," Hyperfine Interact., vol. 117, pp. 271-319, 1998.

[8] S. Zeng, K. Tang, and T. Li, "Controlled synthesis of α-Fe_2O_3 nanorods and its size-dependent optical absorption, electrochemical, and magnetic properties," J. Colloid Interface Sci., vol. 312, pp. 513-521, 2007.

[9] D. Varshney and A. Yogi, "Structural and electrical conductivity of Mn doped hematite (α-Fe_2O_3) phase, " J. Mol. Struct., vol. 995, pp. 157-162, 2011.

[10] C. L. Bruzzone, Ingalls, and R. Mossbauer, "Effect study of the Morin transition and atomic positions in hematite under pressure," Phys. Rev. B, vol. 28, pp. 2430-2440, 1983.

[11] E. Gharibshahian, "The effect of polyvinyl alcohol concentration on the growth kinetics of $KTiOPO_4$ nanoparticles synthesized by the co-precipitation method," HighTech and Innovation Journal, vol. 1, no. 4, pp. 187-193, 2020.

[12] P. H. Kien, Y. Khamphone, and G. T. T. Trang, "Study of effect of size on iron nanoparticle by molecular dynamics simulation," HighTech and Innovation Journal, vol. 2, no. 3, pp. 158-167, 2021.

[13] M. Hosseingholi, "Room temperature synthesis of n-doped urchin-like rutile TiO_2 nanostructure with enhanced photocatalytic activity under sunlight," International Journal of Engineering, Transactions A: Basics, vol. 28, no. 10, pp. 1401-1407, 2015.

[14] N. T. Hahn and C. B. Mullins, "Photoelectrochemical enhancement in Ti- and Sn-doped α-Fe_2O_3 nanostructured photoanodes," Chem. Mater., vol. 22, pp. 6474-6482, 2010.

[15] G. G. Amatucci and N. Pereira, "Fluoride based electrode materials for advanced energy storage devices," J. Fluorine Chem., vol. 128, pp. 243-262, 2007.

[16] T. Mueller, G. Hautier, A. Jain, and G. Ceder, "Evaluation of tavorite-structured cathode materials for lithium-ion batteries using high-throughput computing," Chem. Mater., vol. 23, pp. 3854-3862, 2011.

[17] K.-S. Park, P. Xiao, S.-Y. Kim, A. G. Dylla, Y.-M. Choi, G. Henkelman, et al., "Enhanced charge-transfer kinetics by anion surface modification of $LiFePO_4$," Chem. Mater., vol. 24, no. 16, pp. 3212-3218, 2012, [Online]. Available: https://doi.org/10.1021/cm301569m.

[18] G. G. Amatucci, N. Pereira, T. Zheng, and J.-M. Tarascon, "Failure mechanism and improvement of the elevated temperature cycling of $LiMn_2O_4$ compounds through the use of the $LiAl_xMn_2$-xO_4-zFz solid solution," J. Electrochem. Soc., vol. 148, p. A171, 2001.

[19] S. B. Lee, S. H. Cho, V. Aravindan, H. S. Kim, and Y. S. Lee, " Improved Cycle Performance of Sulfur-Doped LiFePO4 Material at High Temperatures," Bull. Korean Chem. Soc., vol. 30, pp. 2223-2226, 2009.

[20] J. Hu and R. G. Gordon, " Textured fluorine-doped ZnO films by atmospheric pressure chemical vapor deposition and their use in amorphous silicon solar cells," Solar Cells, vol. 30, pp. 437-450, 1991.

[21] M. Eslamian, M. Ahmed, and N. Ashgriz, "Modelling of nanoparticle formation during spray pyrolysis," Nanotechnology, vol. 17, pp. 1674-1685, 2006.

[22] K. Okuyama and I. W. Lenggoro, "Preparation of nanoparticles via spray route," Chem. Eng. Sci., vol. 58, pp. 537-547, 2003.

[23] L. Filipovic, S. Selberherr, G. C. Mutinati, et al., "Modeling spray pyrolysis deposition," vol. 6, 2013.

[24] K. Karthikeyan, S. Amaresh, S. N. Lee, V. Aravindan, and Y. S. Lee, "Fluorine-doped Fe_2O_3 as high energy density electroactive material for hybrid supercapacitor applications," Chem. Asian J., vol. 9, pp. 852-857, 2014.

[25] A. Patterson, "The Scherrer formula for x-ray particle size determination," Phys. Rev., vol. 56, no. 10, pp. 987-982, 1939.

[26] S. S. Chiad, A. S. Alkelaby, and K. S. Sharba, "Optical conduct of nanostructure Co_3O_4 rich highly doping Co_3O_4:Zn alloys," Journal of Global Pharma Technology, vol. 11, no. 7, pp. 662-665, 2020.

[27] P. Malliga, J. Pandiarajan, N. Prithivikumaran, and K. Neyvasagam, "Influence of film thickness on structural and optical properties of sol-gel spin coated TiO_2 thin film," IOSR J. Appl. Phys., vol. 6, pp. 22-28, 2014.

[28] K. H. Kim, K. C. Park, and D. Y. Ma, "Structural, electrical and optical properties of aluminum doped zinc oxide films prepared by rf magnetron sputtering," J. Appl. Phys., vol. 81, p. 7764, 1997.

[29] V. D. Mote, V. R. Huse, and B. N. Dole, "Synthesis and characterization of Cr doped ZnO nanocrystals," World Journal of Condensed Matter Physics, vol. 2, pp. 208-211, 2012.

[30] K. Ozcelik and C. Ergun, "Synthesis, characterization, and antibacterial activity of cobalt doped (α-Fe_2O_3) thin films," Ceram. Int., vol. 41, no. 2, p. 1994, 2015.

[31] S. Shinde, R. Bansode, C. Bhosale, and K. Rajpure, "Physical properties of hematite α-Fe_2O_3 thin films: Application to photoelectrochemical solar cells," Journal of Semiconductors, vol. 32, no. 1, 013001, 2011, doi:10.1088/1674-4926/32/1/013001.

[32] R. Satheesh, K. Vignesh, A. Suganthi, and M. Rajarajan, "Visible light responsive photocatalytic applications of transition metal (M = Cu, Ni and Co) doped α-Fe_2O_3 nanoparticles," Journal of Environmental Chemical Engineering, vol. 2, no. 4, p. 1956, 2014, [Online]. Available: https://pure.atu.ie/en/publications/visible-light-responsive-photocatalytic-applications-of-transitio.

[33] J. Simmons and K. S. Potter, Optical Materials, 1st ed., Academic Press, New York, 1999, [Online]. Available: https://books.google.com/books/about/Optical_Materials.html?id=jeWB-6K5u3EC.

[34] P. E. Agbo and M. N. Nnabuchi, "Growth and optical properties of nanocrystalline CdS thin films prepared by spray pyrolysis," Chalcogenide Letters, vol. 8, p. 273, 2011.

[35] Y. A. AL Shaabani, "Studying some physical properties of Zn_2xCu_1-xIn_1-xS_2 thin films prepared by chemical spray pyrolysis," Applied Sciences University of Technology, 2009.

[36] R. S. Ali, M. K. Mohammed, A. A. Khadayeir, Z. M. Abood, N. F. Habubi, and S. S. Chiad, "Structural and optical characterization of sprayed nanostructured indium doped Fe_2O_3 thin films," J. Phys.: Conf. Ser., vol. 1664, no. 1, 012016, 2020.

[37] M. Matsuoka, M. Kitano, M. Takeuchi, K. Tsujimaru, M. Anpo, and J. M. Thomas, "Photocatalysis for new energy production: Recent advances in photocatalytic water splitting reactions for hydrogen production," Catal. Today, vol. 122, p. 51, 2007, doi:10.1016/j.cattod.2007.01.042.

[38] A. A. Khadayeir, R. I. Jasim, S. H. Jumaah, N. F. Habubi, and S. S. Chiad, "Influence of substrate temperature on physical properties of nanostructured ZnS thin films," J. Phys.: Conf. Ser., vol. 1664, no. 1, 2020.

[39] S. Wang, W. Wang, W. Wang, Z. Jiao, J. Liu, and Y. Qian, "Characterization and gas-sensing properties of nanocrystalline iron (III) oxide films prepared by ultrasonic spray pyrolysis on silicon," Sensors and Actuators B: Chemical, vol. 69, pp. 22-27, 2000.

[40] E. Lee, G. Jang, C. Kim, and D. Yoon, "Fabrication and gas sensing properties of α-Fe_2O_3 thin film prepared by plasma enhanced chemical vapor deposition (PECVD)," Sensors and Actuators B: Chemical, vol. 77, pp. 221-227, 2001.

[41] Q. Hao, L. Li, X. Yin, S. Liu, Q. Li, and T. Wang, "Anomalous conductivity-type transition sensing behaviors of n-type porous α-Fe_2O_3 nanostructures toward H_2S," Mater. Sci. Eng. B, vol. 176, pp. 600-605, 2011.

[42] K. L. Hardee and A. J. Bard, "Semiconductor electrodes. 10. Photoelectrochemical behavior of several polycrystalline metal-oxide electrodes in aqueous solutions," J. Electrochem. Soc., vol. 124, p. 215, 1977.

[43] H. T. Salloom, E. H. Hadi, N. F. Habubi, S. S. Chiad, M. Jadan, and J. S. Addasi, "Characterization of silver content upon properties of nanostructured nickel oxide thin films," Digest Journal of Nanomaterials and Biostructures, vol. 15, no. 4, pp. 1189-1195, 2020.

[44] R. S. Ali, N. A. H. Al Aaraji, E. H. Hadi, K. H. Abass, N. F. Habubi, and S. S. Chiad, "Effect of lithium on structural and optical properties of nanostructured CuS thin films," Journal of Nanostructures, vol. 10, no. 4, pp. 810-816, 2020.

[45] A. Z. Moshfegh, R. Azimirad, and O. Akhavan, "Optical properties and surface morphology of evaporated $(WO_3)_1$-x–(Fe_2O_3)x thin films," Thin Solid Films, vol. 484, pp. 124-131, 2005.

[46] J. A. Glasscock, P. R. F. Barnes, I. C. Plumb, and N. Savvides, "Enhancement of photoelectron chemical hydrogen production from hematite thin films by the introduction of Ti and Si," J. Phys. Chem. C, vol. 111, pp. 16477-16488, 2007.

[47] A. K. Varshneya, Fundamentals of Inorganic Glasses, Academic Press Inc., San Diego, 1994.

[48] W. Wenjian, M. Ma, P. Du, Z. Gaoling, G. Shen, J. Wang, and G. Han, "Superhydrophilic Fe doped titanium dioxide thin films prepared by a spray pyrolysis deposition," Surf. Coat. Technol., vol. 198, pp. 340-344, 2005.

[49] E. F. Keskenler, G. Turgut, and S. Dogan, "Investigation of structural and optical properties of ZnO films co-doped with fluorine and indium," Superlattices Microstruct., vol. 52, pp. 107-115, 2012.

[50] J. I. Pankov, Optical Processes in Semiconductors, 1971.

[51] J. Kaur and M. Sharma, "Structural and optical studies of undoped and copper doped zinc sulphide nanoparticles for photocatalytic application," Superlattices Microstruct., vol. 77, pp. 35-53, 2015.

[52] M. A. Kaid and A. Ashour, "Preparation of ZnO-doped Al films by spray pyrolysis technique," Appl. Surf. Sci., vol. 253, pp. 3029-3033, 2007.

[53] U. Schwertmann, R. W. Fitzpatrick, R. M. Taylor, and D. G. Lewis, "The influence of aluminum on iron oxide. Part II. Preparation and properties of Al-substituted hematites," Clays Clay Miner., vol. 27, no. 2, pp. 105-112, 1979.

[54] D. G. Schulze and U. Schwertmann, "The influence of aluminum on iron oxides. XIII. Properties of goethites synthesized in 0.3 M KOH at 25°C," Clay Miner.,
vol. 22, pp. 83-92, 1987.

[55] M. R. Belkhedkar, A. U. Ubale, Y. S. Sakhare, N. Zubair, and M. Musaddique, "Characterization and antibacterial activity of nanocrystalline Mn doped Fe_2O_3 thin films grown by successive ionic layer adsorption and reaction method," Journal of the Association of Arab Universities for Basic and Applied Sciences, vol. 21, pp. 38-44, 2016.

[56] Y. H. Elbashar and H. A. Abd El-Ghany, "Optical spectroscopic analysis of Fe_2O_3 doped CuO containing phosphate glass," Opt. Quant. Electron., vol. 49, p. 310, 2017.

[57] J. H. Park, S. Kim, and A. J. Bard, "Novel carbon-doped TiO_2 nanotube arrays with high aspect ratios for efficient solar water splitting," Nano Letters, vol. 6,
p. 24, 2006, [Online]. Available: http://bard.cm.utexas.edu/styled-5/styled-26/

[58] K. G. Mor, H. E. Prakasam, O. K. Varghese, K. Shankar, and C. A. Grimes, "High-aspect-ratio TiO_2 nanotube arrays prepared by anodic oxidation of titanium," Nano Letters, vol. 7, no. 8, pp. 2356–2364, 2007.

[59] C. D. Park, D. Magana, and A. E. Stiegman, "High-quality Fe and γ-Fe_2O_3 magnetic thin films from an epoxide-catalyzed sol–gel process," Chemistry of Materials, vol. 19, pp. 677–683, 2007.

[60] X. W. Li, A. Gupta, G. Xiao, and G. Q. Gong, "Transport and magnetic properties of epitaxial and polycrystalline magnetite thin films," Journal of Applied Physics, vol. 83, pp. 7049–7051, 1998.